Journal of Hydraulic Research

ISSN: 0022-1686 (Print) 1814-2079 (Online) Journal homepage: https://www.tandfonline.com/loi/tjhr20

Experimental study of dam-break flow against an isolated obstacle

S. Soares-Frazão & Y. Zech

To cite this article: S. Soares-Frazão & Y. Zech (2007) Experimental study of dam-break flow against an isolated obstacle, Journal of Hydraulic Research, 45:sup1, 27-36, DOI: 10.1080/00221686.2007.9521830

To link to this article: https://doi.org/10.1080/00221686.2007.9521830

Journal of Hydraulic Research Vol. 45 Extra Issue (2007), pp. 27–36

Experimental study of dam-break flow against an isolated obstacle

Impact d'un obstacle isolé sur l'écoulement consécutif à une rupture de barrage : mesures expérimentales

S. SOARES-FRAZÃO, *Fonds National de la Recherche Scientifique and Department of Civil and Environmental Engineering, Université catholique de Louvain, Belgium. E-mail: soares@gce.ucl.ac.be*

Y. ZECH, *Department of Civil and Environmental Engineering, Université catholique de Louvain, Belgium. E-mail: zech@gce.ucl.ac.be*

ABSTRACT
During a dam-break flow, the whole valley is involved, which implies that roads, bridges and urban buildings become obstacles to the flow. The purpose of this paper is to provide data about the influence of such an obstacle on a dam-break wave, the obstacle being an idealised representation of a single building. The experimental set-up consists in a channel with a rectangular shaped obstacle, representing a building, placed immediately downstream from the dam. The building is neither centred in the channel, nor aligned with the flow direction. Flow observation shows that after the violent impact of the wave on the building, the flow is forced to change its direction to pass the building. This implies the formation of hydraulic jumps with the consequence that the water level may rise locally higher than without building. Behind the building, a wake zone is observed. Then, further downstream, the flow slowly recovers the structure it would have had without the building. Several measurement devices were used to characterise the flow. At five different locations, the water level evolution was measured by means of water level gauges while the velocity was measured by means of an acoustic Doppler velocimeter. Then, the surface velocity field was obtained using digital imaging techniques.

RÉSUMÉ
Lors d'écoulements consécutifs à une rupture de barrage, la vallée entière est concernée. Les routes, ponts et bâtiments divers deviennent donc des obstacles à l'écoulement. Le présent article a pour but d'étudier l'influence d'un tel obstacle sur l'écoulement, l'obstacle étant représenté de manière idéalisée par un bâtiment isolé. Le dispositif expérimental consiste en un canal dans lequel on a placé un obstacle de forme rectangulaire à l'aval immédiat du barrage. L'obstacle n'est pas centré dans le canal, ni aligné avec la direction principale de l'écoulement. Les observations montrent que, après l'impact violent de l'onde de rupture de barrage sur l'obstacle, l'écoulement doit changer de direction pour contourner le bâtiment. Cela implique la formation de ressauts hydrauliques avec pour conséquence un niveau d'eau localement beaucoup plus élevé que s'il n'y avait pas de bâtiment. Derrière l'obstacle, on observe une zone de sillage. Ensuite, plus loin vers l'aval, l'écoulement recouvre progressivement l'aspect qu'il aurait eu sans la présence de l'obstacle. Divers instruments de mesure ont été utilisés pour caractériser l'écoulement. Les hauteurs d'eau ainsi que les vitesses ont été mesurées à cinq endroits, au moyen respectivement de capteurs résistifs et de sondes acoustiques Doppler. Enfin, le champ de vitesses de surface a été mesuré au moyen de techniques d'imagerie digitale.

Keywords: Dam-break flow, experiments, obstacle, ADV velocity measurements, digital imaging velocity measurements.

1 Introduction

This paper presents a test case aimed at investigating the effects of a single building on a dam-break flow. It is part of the broader study of flood propagation in urban areas undertaken during the IMPACT project (IMPACT, 2004). The data set presented in this paper was used within the frame of the IMPACT project as a benchmark aimed at validating numerical models designed for solving severe transient flow problems in complex topographies (Soares-Frazão *et al.*, 2003).

The presence of obstacles is common in river as well in main channel (bridge piers) as in floodplains (abutments, dikes, trees and vegetation, debris from former floods, etc.). Moreover, if the river embankments are overtopped or the flood dikes breached, flow will invade areas that are normally not subject to inundation, not prepared to support such a hazard, and thus presenting a series of obstacles (roads, railways, dwellings, industrial and commercial structures, etc.).

Flows may be considerably affected by the presence of such natural or artificial obstacles. In the case of severe floods, for example due to dam- or dike-break, the influence of such obstacles is even amplified, especially in the first instants after the dam break and at the immediate vicinity of the dam.

Revision Received July 26, 2006/Open for discussion until August 31, 2007.

Two simplified approaches are generally used to represent the influence of an obstacle on the flow: they are considered as inducing either a reduced flow conveyance or an increased bed friction slowing down the wave propagation. But those approaches are not able to produce accurate predictions under severe transient flow conditions. Indeed, the flow route can be modified, and the flood wave can reflect against the obstacle, increasing the upstream water depths dramatically.

In this paper, the impact of a dam-break flow on an obstacle was investigated in the laboratory using a single building placed in a channel, immediately downstream from the gate simulating the dam.

2 Experimental set-up

The experiments were carried out in the Civil Engineering Laboratory of the Université catholique de Louvain (UCL) in Belgium. Preliminary results of this investigation can be found in Soares-Frazão *et al.* (2004).

The channel and building dimensions are indicated in Fig. 1. The channel is about 36 m long, with a rectangular cross section except near the bed, where this section is cut to form a trapezoidal shape (Fig. 2a). A gate separates the upstream part of the channel, representing the reservoir, from the downstream part, representing the valley. The gate is located between two impermeable fixed blocks and the cross section between those abutments is rectangular and narrower than the channel cross-section (Fig. 2b). The channel bed is horizontal. From former experiments in this facility, a Manning friction coefficient was estimated to $n = 0.010\,\mathrm{sm}^{-\frac{1}{3}}$.

The location and dimensions of the building are indicated in Fig. 1. The exact co-ordinates of the four corners of the building according to the origin of the axes are indicated in Table 1. The origin of the axes is taken at the centre of the gate, with positive x-direction towards the downstream end of the channel (Fig. 1).

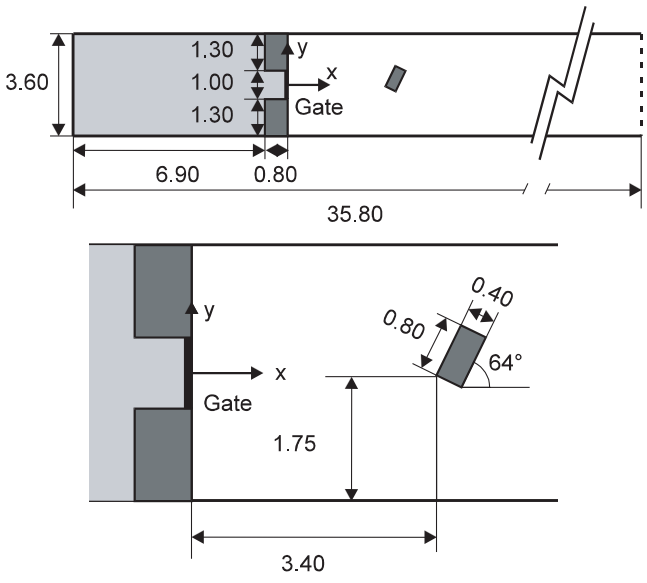

Figure 1 Channel and building dimensions (m).

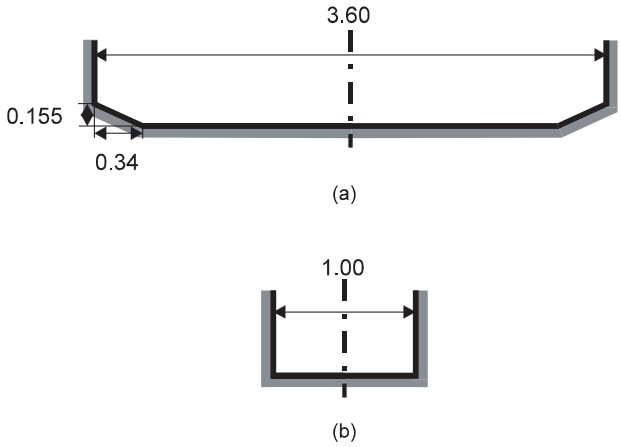

Figure 2 Cross section (a) in the channel and in the reservoir and (b) at the dam location.

Table 1 Co-ordinates of the building corners

	x (m)	y (m)
Corner 1	3.44	−0.05
Corner 2	3.80	−0.23
Corner 3	4.15	0.49
Corner 4	3.79	0.67

The initial conditions for the experiment consist in a water depth in the upstream reservoir $h_0 = 0.40$ m and a thin layer of 0.02 m of water in the channel. To simulate the dam break, the gate separating the reservoir from the channel is pulled up rapidly, resulting in an instantaneous dam break. Indeed, the gate opening time for this experiment is 0.23 s. This time can be compared to the criterion established by Vischer and Hager (1998), stating that a dam break can be considered as instantaneous if the gate opening time t_{op} satisfies the following relationship, with $h_0 = 0.4$ m

$$t_{op} \leq 1.25\sqrt{\frac{h_0}{g}} = 0.25\,\mathrm{s} \tag{2.1}$$

In the present case, $t_{op} = 0.23$ s, the criterion is thus satisfied. Another criterion was developed by Lauber and Hager (1998a, b), stating that

$$t_{op} \leq \sqrt{\frac{2\,h_0}{g}} = 0.29\,\mathrm{s} \tag{2.2}$$

This latter criterion is less restrictive, and is thus also satisfied.

The upstream end of the channel (which is also the upstream end of the reservoir, at $x = -7.70$ m) is a closed wall. At the far downstream end of the channel (i.e. 29 m from the gate), there is a sediment settling system making this boundary an unclear combination of weirs and walls. However, it was observed that there is no influence of this boundary condition during the first 30 seconds after the dam break. Any downstream boundary condition may thus be imposed in numerical models provided that the imposed downstream boundary condition does not influence the flow throughout the duration of the modelling.

3 Flow description

Following the rapid opening of the gate, the strong dam-break wave reflects against the building, and the flow separates, forming a series of shock waves crossing each other. A wake zone can be identified just downstream from the building, surrounded by cross waves. After a fast transient phase, the flow features a slower evolution, following the progressive emptying of the reservoir. Also, re-circulation zones can be identified between the building and the walls.

This description of the flow is illustrated by means of Figs. 3–5. For seek of clarity, these are not immediately gained from experiments, but from computed results (Noël *et al.*, 2003), which have been compared successfully to the measurements (Soares-Frazão *et al.*, 2003), in such a way that they provide a good overview of the flow features. Figure 3 shows the free-surface elevation at $t = 1$ s, clearly featuring the two-dimensional spreading of the flood wave.

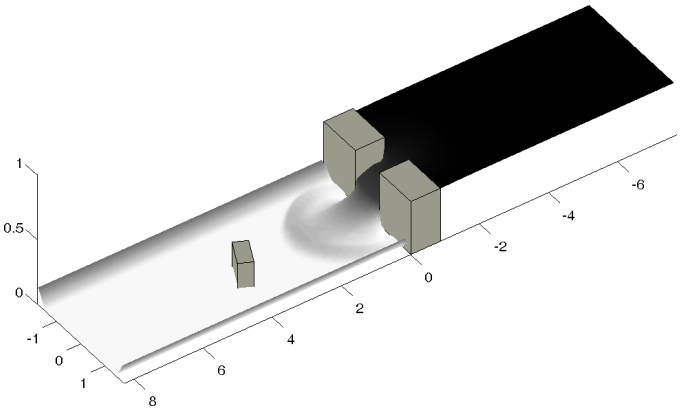

Figure 3 Computed image of the flow at time $t = 1$ s.

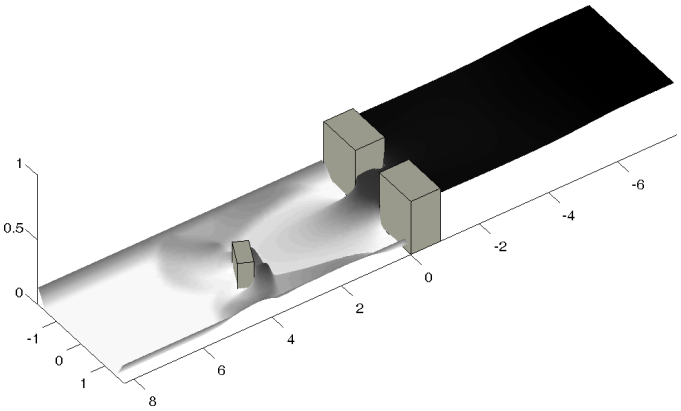

Figure 4 Computed image of the flow at time $t = 3$ s.

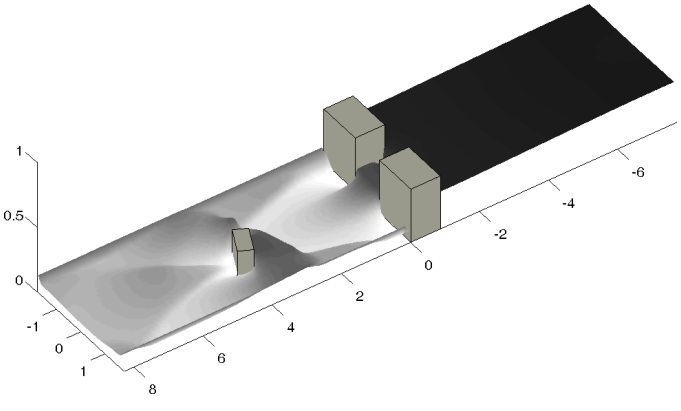

Figure 5 Computed image of the flow at time $t = 10$ s.

At $t = 3$ s, the reflection of the wave against the building has occurred and results in the formation of an oblique hydraulic jump (Fig. 4). The circular front wave also reflects against the side walls of the channel and lateral jumps are formed. Figure 5 shows the flow after 10 s: the hydraulic jump formed by the reflection against the building recedes in the upstream direction. The separation of the flow around the building and the wake zone can also be identified.

4 Flow measurement

Three types of measurements were undertaken. At several gauging stations, the time evolution of the water level and of the velocity was measured using resistive gauges and Acoustic Doppler Velocimeters (ADV), respectively. Both devices are intrusive and it could be feared they alter the flow to be measured. However, it was noted that the perturbation so induced remains local and that the measurements match the visual observations. Besides, to circumvent the intrusive nature of those devices, alternative measurements of the velocity were carried out using digital imaging techniques (Capart *et al.*, 2002, Spinewine *et al.*, 2003), in order to obtain the surface-velocity field in the area around the building. Velocities measured using this last technique were compared to velocities measured using ADV probes at the gauging points.

4.1 Depth and velocity measurements at some points

The water level is measured by means of 6 water-level gauges located in the channel as indicated in Fig. 6: one gauge in the reservoir to monitor its emptying and thus the inflow discharge,

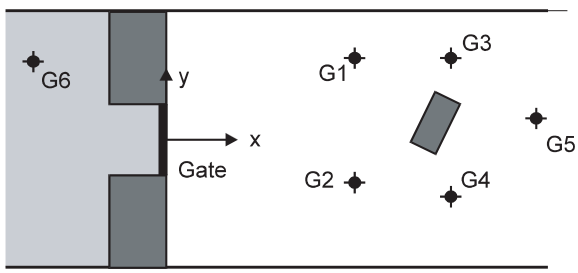

Figure 6 Sketch of the location of the gauging points where the water level and the velocity are measured.

Table 2 Position of the gauges

Gauge	x (m)	y (m)
G1	2.65	1.15
G2	2.65	−0.60
G3	4.00	1.15
G4	4.00	−0.80
G5	5.20	0.30
G6	−1.87	1.10

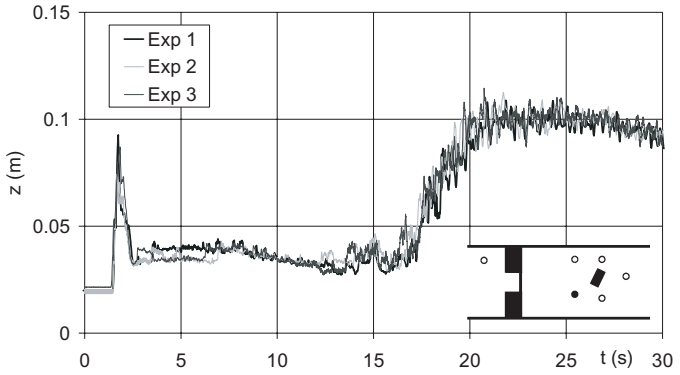

Figure 7 Repeatability of gauge measurements at gauge G2.

and the others around the building. Their exact position is given in Table 2.

The experiment was run several times and showed a very good repeatability, as illustrated in Fig. 7 for three different runs of the experiment, at gauge G2.

The velocity was also measured at the same locations by means of an ADV. However, no complete vertical velocity profiles were measured. Only one velocity data was measured at each gauging point, at a height of 3.6 cm above the channel bed to ensure that the transducers remained submerged during the major part of the experiment. As the flow is a rapid transient with hydraulic jumps and re-circulation zones, the velocity distribution is quite complex and varies in time. The ADV measurements are used to assess the validity of surface-velocity measurements by digital imaging. This will be detailed in Section 4.3.

4.2 Velocity-field measurements

A complete surface-velocity field was measured by a digital imaging technique. High-resolution CCD cameras were placed above the channel to capture the flow seeded with tracers, at a rate of 38 frames per second. This results in a series of images where the white tracers can be clearly identified. Using the Voronoï technique (Capart *et al.*, 2002; Spinewine *et al.*, 2003) to reconstruct the trajectories of the tracers on the free surface, it was possible to obtain measurements of the velocity field at the free surface.

Thanks to the good repeatability of the experiment, it was possible to combine the resulting images from several runs and thus to cover a large area of the channel. Such a combination of filmed images is shown in Fig. 8. Cross marks correspond to the position of the gauging points and the white tracers can also be identified in the figure.

4.3 Validity of velocity measurements

By means of the ADV probe, the velocity components u and v in the x and y directions respectively were obtained at a constant level 3.6 cm above the channel bed. The digital imaging technique provides the surface velocity. Both are distinct from the depth-averaged velocity in fully developed flows. In the present situation of fast transient flows, no conclusions can be drawn

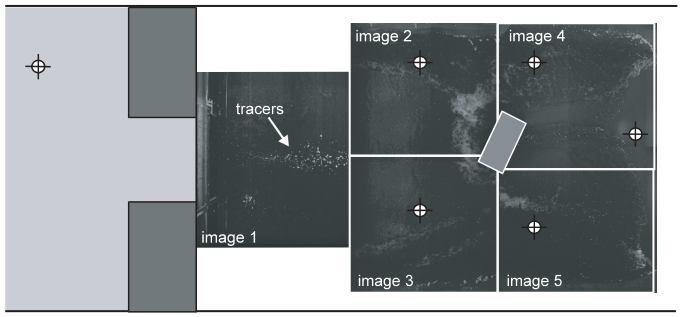

Figure 8 Combination of filmed images from five experiments to cover a whole field around the building ($t = 1.2$ s).

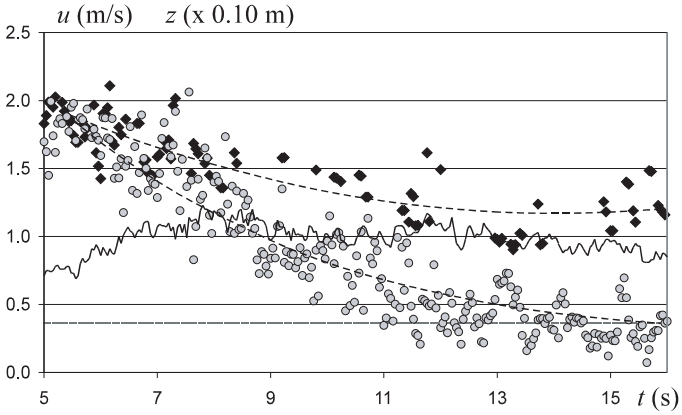

Figure 9 Gauge G1—Water level h (continuous black line) and ADV probe level z_0 (dashed grey line) with a scale unit of 10 cm; velocity measurements (grey marks = ADV measurements u_0; black marks = surface velocities u_s, the scale unit is 1 m/s, dotted lines give the polynomial regressions).

regarding the velocity profile: at some moments, at some locations, the flow is close to a fully developed flow, featuring a log or a wake-log vertical distribution. But this profile can evolve in time and space to the point of sometimes presenting a reverse distribution (lower velocity at the free surface than close to the bed), as might happen for example in a steady hydraulic jump. Moreover, it must be kept in mind that, depending on the local water depth, the ADV probe is sometimes close to the free surface and sometimes below the mid depth. The particular situation of each of the five gauging points is investigated in this section.

For gauge G1, the results are presented in Fig. 9, where different measurements were combined to illustrate the discussion. The measured water depth h (continuous black line) and the probe level z_0 (dotted grey line) are indicated (scaled by a factor 10, for the clarity of the figure), and it can be observed that the ADV probe is always well submerged, which is a necessary condition to obtain valuable measurements. The rough velocity measurements obtained by means of the ADV probe (u_0, grey marks) and by means of digital imaging (u_s, black marks) are indicated. Although there is an important scatter of the data, a general trend can be observed, that is highlighted by a polynomial regression of each data set (dotted black lines). The surface velocity, denoted u_s, and the velocity at $z_0 = 0.036$ m, measured by the ADV probe and denoted u_0, are close to each other at $t = 5$ s. Later, u_0 reduces more rapidly than u_s.

Based on the experimental data (polynomial regression for the velocities), log and wake-log laws were calculated at different times to check the velocity profiles. Four profiles were calculated at each considered time: a log and a wake-log law passing through the point (z_0, u_0) and a log and a wake-log law passing through the point (h, u_s). The log law distribution reads (see e.g. Graf and Altinakar, 1998)

$$u = u_s + \frac{u_*}{\kappa} \ln\left(\frac{z}{h}\right) \tag{4.1}$$

while the wake log law may be expressed for instance in the following form (Graf and Altinakar, 1998):

$$u = u_s + \frac{u_*}{\kappa} \ln\left(\frac{z}{h}\right) - u_* \frac{2\,\Pi}{\kappa}\left[1 - \sin^2\left(\frac{\pi}{2}\frac{z}{h}\right)\right] \tag{4.2}$$

where u_s denotes the velocity at the free surface, u_* is the shear velocity, Π is Coles' factor whose average value is 0.2 (Graf and Altinakar, 1998) and κ is von Kárman's constant. Equations (4.1) and (4.2) are used to calculate the profiles passing through the surface imaging-measured point (h, u_s).

For the profiles passing through the ADV-measured point (z_0, u_0), u_s can be calculated for the log and wake-log laws respectively as

$$u_s = u_0 - \frac{u_*}{\kappa} \ln\left(\frac{z_0}{h}\right) \tag{4.3}$$

$$u_s = u_0 - \frac{u_*}{\kappa} \ln\left(\frac{z_0}{h}\right) + u_* \frac{2\,\Pi}{\kappa}\left[1 - \sin^2\left(\frac{\pi}{2}\frac{z_0}{h}\right)\right] \tag{4.4}$$

The theoretical velocity profiles calculated by (4.1) and (4.2) are compared to the measurements in Fig. 10, at times $t = 5.5$ s, 10 s and 14 s, respectively.

At time $t = 5$ s, both log and wake-log theoretical profiles give velocities widely spread over the depth, while the two measured points appear to be aligned on a vertical line, which would indicate that the profile is rather uniform at this time. At later times, the surface velocity u_s is much larger than the velocity u_0 measured by the ADV probe. It would be hazardous to deduce a correction factor to be applied to the surface velocity in order to transform it into depth-averaged velocity. Moreover, it might be assumed that the surface-velocity measurements, based on the tracer positions, could be affected at some locations by the important local slopes of the free surface, which could dissociate the tracer from the water velocity. The surface-velocity data set is thus to be handled with care.

For gauge G2, the ADV velocity measurements can be used only from time t = 14.5 s, as before, the probe is not sufficiently submerged. This is illustrated in Fig. 11: the flow is supercritical, with a low water depth and a high velocity. However, it can also be observed that both velocity data sets have a small scatter and follow the same trend, which might lead to consider them both as valid measurements. The ADV measurement is probably affected by the position of the probe, very close to the free surface, which could explain the constant lag observed in the measurements.

For gauge G3, the same procedure as for gauge G1 was used: polynomial curves were fitted through the measured velocities (Fig. 12), then a log and a wake-log law were calculated in order to pass through the measured points u_0 and u_s, respectively.

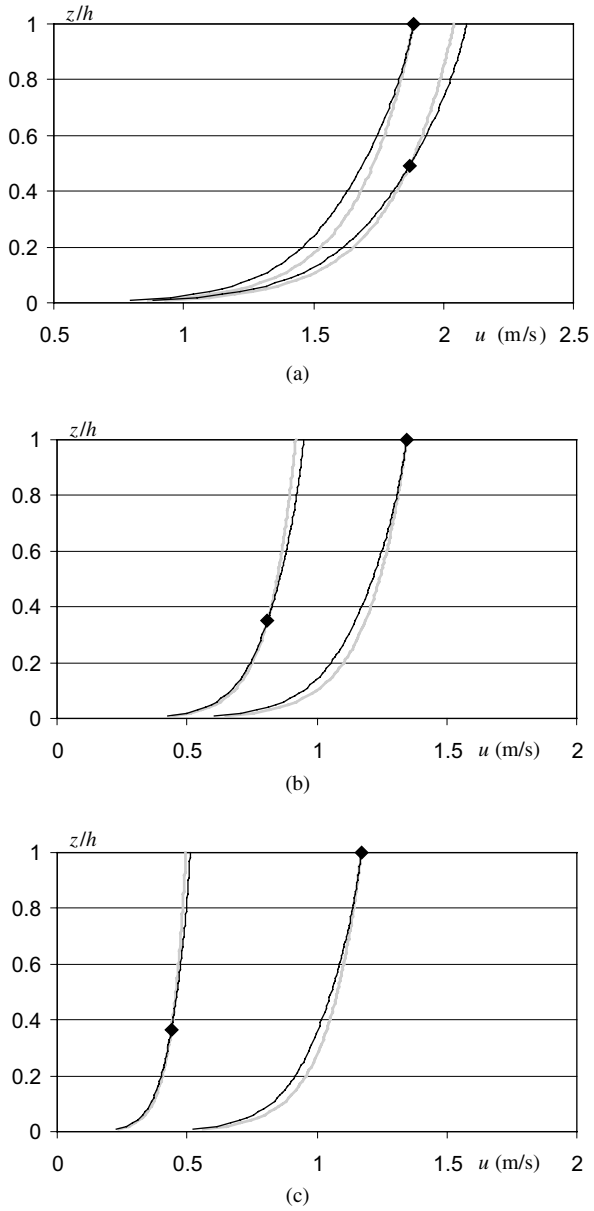

Figure 10 Gauge G1—Log law (black line) and wake-log law (grey line) velocity profiles passing through u_0 or u_s (♦) at times (a) 5.5 s, (b) 10 s and (c) 14 s.

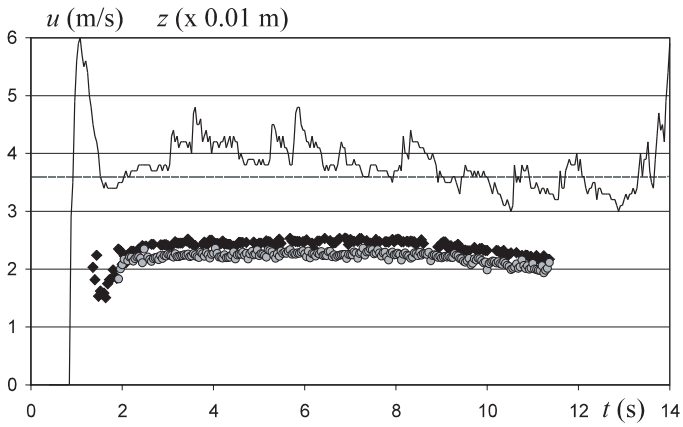

Figure 11 Gauge G2—Water level h (continuous black line) and ADV probe level z_0 (dashed grey line) with a scale unit of 1 cm; Velocity measurements (grey marks = ADV measurements u_0; black marks = surface velocities u_s, the scale unit is 1 m/s).

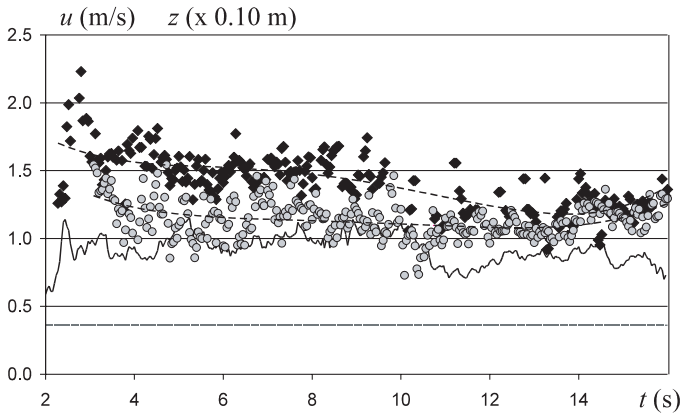

Figure 12 Gauge G3—Water level h (continuous black line) and ADV probe level z_0 (dashed grey line) with a scale unit of 10 cm; and velocity measurements (grey marks = ADV measurements u_0; black marks = surface velocities u_s, the scale unit is 1 m/s, dotted lines give the polynomial regressions).

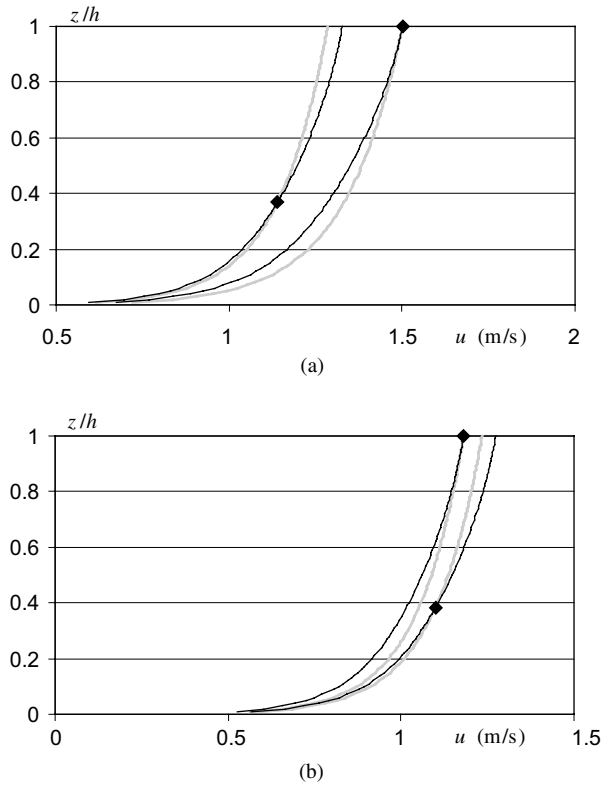

Figure 13 Gauge G3—Log law (black line) and wake-log law (grey line) velocity profiles passing through u_0 or u_s (♦) at times (a) 7 s and (b) 14 s.

Both velocity data sets follow a similar trend, and they get closer to each other from time $t = 12$ s. Velocity profiles at times $t = 7$ s and 14 s are compared in Fig. 13. At time t = 14 s, the measured velocities seem to be close to a uniform profile, but could also be positioned on a profile of the log type. At earlier times, the measured surface velocity is larger than the prediction by the wake log law and the actual profile is certainly not uniform.

At the location of gauge G4 (Fig. 14), the ADV probe is also well submerged. The polynomial regression of both velocity data sets yields two curves that follow a similar decreasing trend between times $t = 6$ s and $t = 16$ s. It is interesting to note how the velocity is out-of-phase with the water level: the

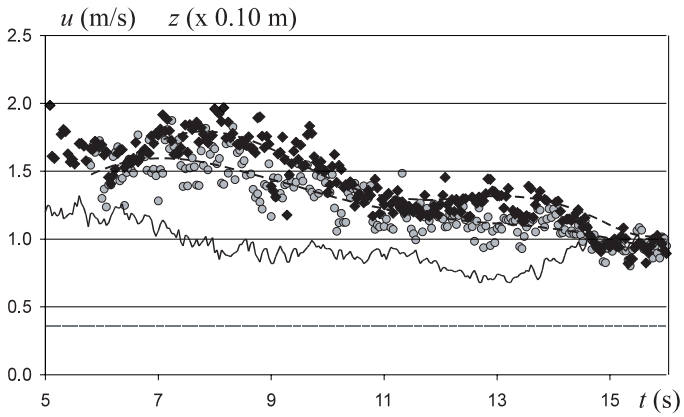

Figure 14 Gauge G4—Water level h (continuous black line) and ADV probe level z_0 (dashed grey line) with a scale unit of 10 cm; and velocity measurements (grey marks = ADV measurements u_0; black marks = surface velocities u_s, the scale unit is 1 m/s, dotted lines give the polynomial regressions).

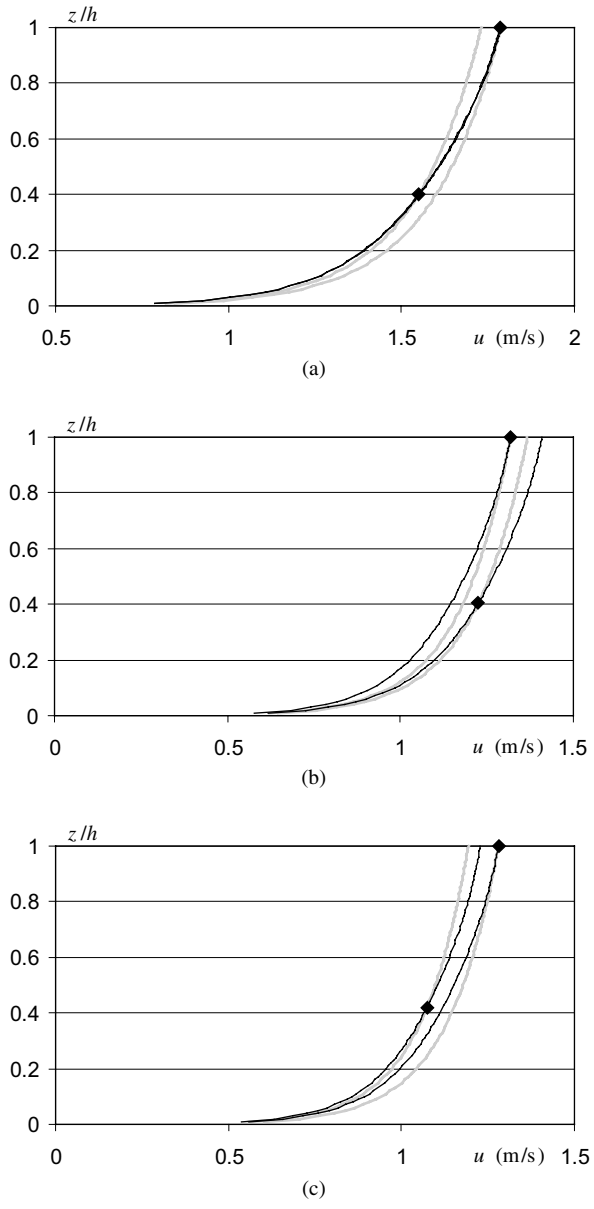

Figure 15 Gauge G4—Log law (black line) and wake-log law (grey line) velocity profiles passing through u_0 or u_s (♦) at times (a) 8 s, (b) 11 s and (c) 14 s.

velocity increases when the water level decreases and decreases when the water level increases. It must also be kept in mind that the discharge is globally decreasing as the flow is the result of a dam break.

Again, the validity of a log law or wake-log law profile was checked. The results are shown in Fig. 15. At time $t = 8$ s, the wake-log law fitted through u_s and through u_0 agree, which validates this profile. This is less clear for subsequent times: the velocity is slightly more uniform at $t = 11$ s and a little less at time $t = 14$ s, respectively.

Finally, the results at gauge G5 are more difficult to interpret. The ADV probe is well submerged, but all velocity measurements show an important scatter. This is due to the position of the gauge, in the wake zone of the building. Those results are analysed in Section 5.3.

5 Experimental results

Some examples of experimental results available for this test case are presented here under the form of graphs and plots. The detailed test data can be found in the attached DVD-ROM.

5.1 Digital imaging measurements

By tracking the tracers on the combined filmed images and applying the Voronoï technique developed by Capart *et al.* (2002) and Spinewine *et al.* (2003), surface-velocity fields are obtained as shown in the following figures. The randomly located measured velocities arising from the tracking of individual particles were mapped onto a square grid, where errors emanating from lightening contrasts were eliminated.

Figure 16 shows the flow at $t = 1$ s. The two-dimensional spreading of the front wave is clearly visible. Then, at $t = 2$ s (Fig. 17), the front reaches both building and the inclined side walls of the channel where a first reflection occurs. This reflection appears in the figure as a sudden change in direction and amplitude of the velocity vectors.

At time $t = 5$ s (Fig. 18), the hydraulic jumps formed by the reflection of the front wave against the building can be identified as the limit between high velocities upstream from the building and an area of water almost at rest. The lateral hydraulic jumps

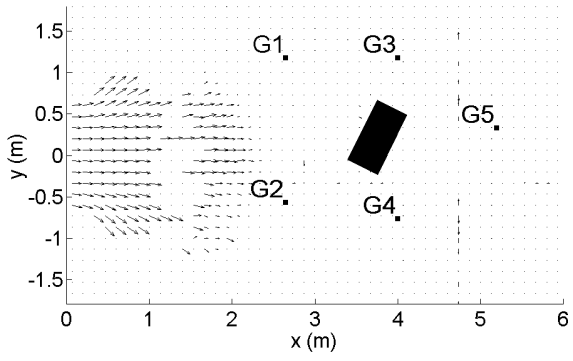

Figure 16 Measured velocity field at $t = 1$ s.

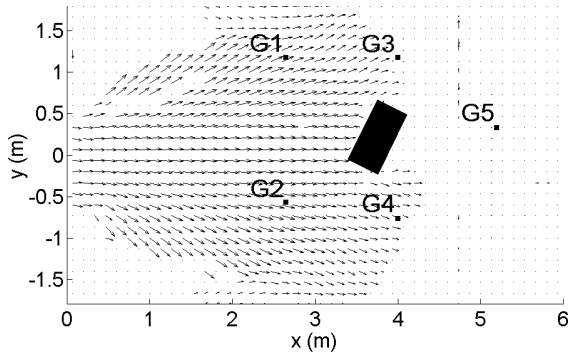

Figure 17 Measured velocity field at $t = 2$ s.

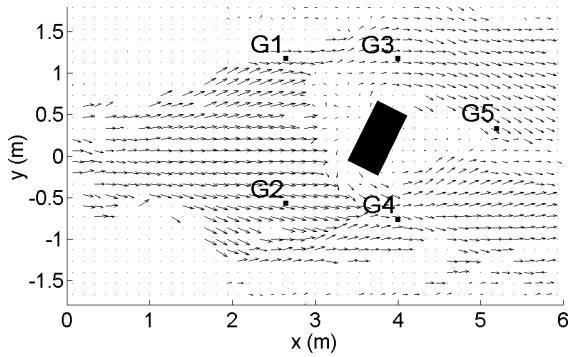

Figure 18 Measured velocity field at $t = 5$ s.

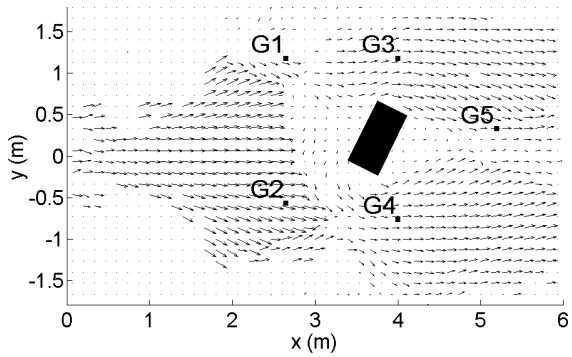

Figure 19 Measured velocity field at $t = 10$ s.

are still present. The flow separates to pass around the building and a wake is formed behind this.

Those latter features then remain and attenuate while the flow reaches a slowly evolving state as the upstream reservoir empties. Figure 19 shows the velocity field after 10 s: the hydraulic jump has propagated slowly in the upstream direction, the wake zone is still present but the velocities have decreased in amplitude.

5.2 Water-level measurements at gauging points

The points where the water level was measured are indicated in Fig. 6. Gauge G6, located in the upstream reservoir, shows a progressive decrease of the water level as the reservoir empties (Fig. 20). Oscillations of the free surface in the reservoir occur as the back wave reaches the different borders of the reservoir at different times and are reflected, resulting in a superposition of smooth waves.

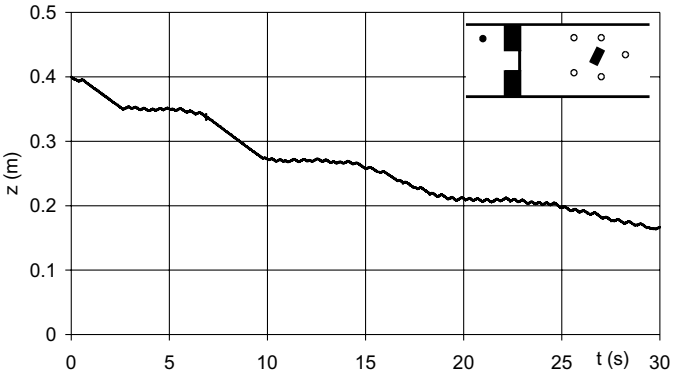

Figure 20 Water level evolution at gauge G6.

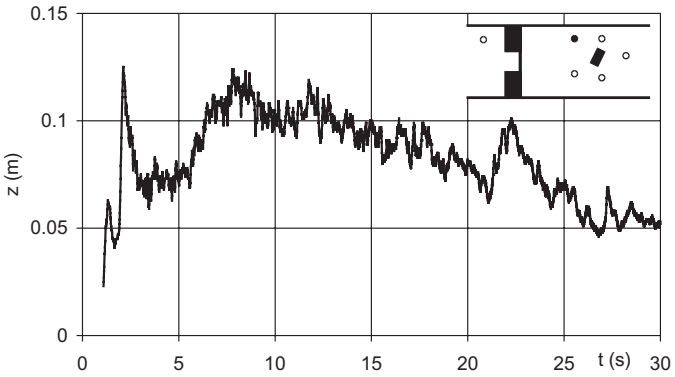

Figure 21 Water level evolution at gauge G1.

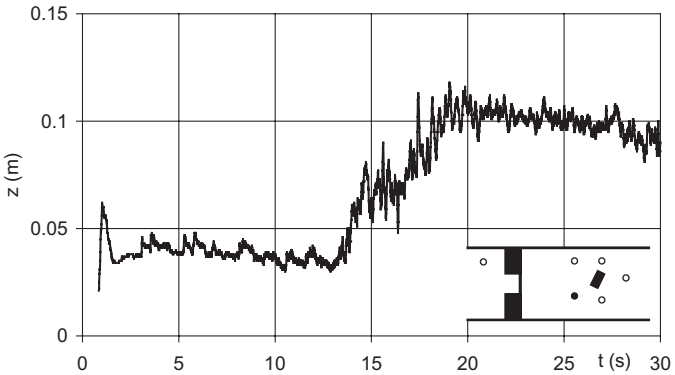

Figure 22 Water level evolution at gauge G2.

Gauge G1 (Fig. 21) is located upstream from the building and close to the left bank of the channel. The water level rapidly rises due to reflection of the front wave against the inclined bank of the channel, appearing as a "splash" in the gauge measurements. Then, around $t = 8$ s, the oblique hydraulic jump formed by the reflection against the banks reaches the gauge.

The main hydraulic jump formed by the reflection of the wave against the building is well captured by gauge G2 (Fig. 22) around $t = 15$ s.

Gauge G4 (Fig. 23), located on the right side of the building, records several reflections of the flow. First, there is a kind of "splash" effect at $t = 2.5$ s due to the strong reflection of the water against the building. Then, the arrival of the oblique hydraulic jump formed by the reflection of the front wave against the right side wall of the channel ($t = 5$ s) can be observed. Finally a new rise of the water level is observed (around $t = 15$ s) when the

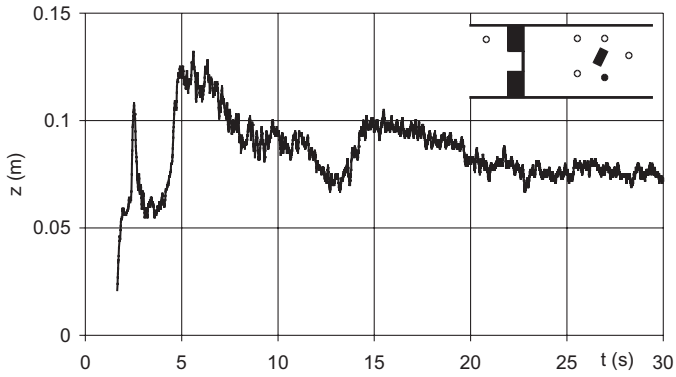

Figure 23 Water level evolution at gauge G4.

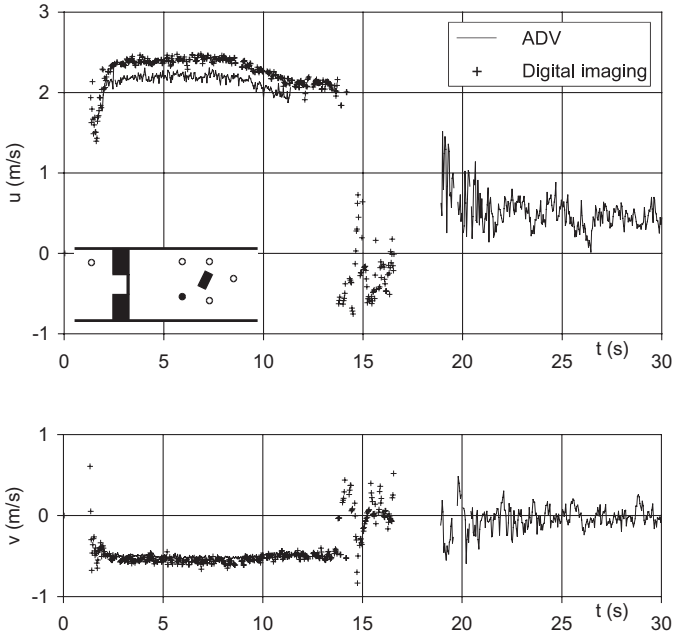

Figure 24 Gauge G2—Velocity measurements.

oblique hydraulic jump and the main hydraulic jump merge and start moving in the upstream direction.

5.3 Velocity measurements at gauging points

The validity and limitations of both measurements techniques (ADV and digital imaging) have already been outlined in Section 4.3.

The velocity measurements at gauge G2 (Fig. 24) illustrate the change from supercritical flow to subcritical flow around $t = 15$ s through a hydraulic jump. This jump could already be observed in Fig. 22, giving the evolution of the water level at G2. During the supercritical period, the velocity magnitude is important (around $2\,\mathrm{m\,s^{-1}}$). The u-component is predominant, and the v-component shows that the flow is spreading from the gate in the direction of the gauge. Then, after the passage of the hydraulic jump, the velocity magnitude decreases to a value around $0.5\,\mathrm{m\,s^{-1}}$ and the v-component practically vanishes, which indicates that the flow is now mainly one-dimensional.

At gauge G4 (Fig. 25), a change in direction and in the velocity magnitude can also be observed around $t = 15$ s, corresponding to a rise of the water level (Fig. 23).

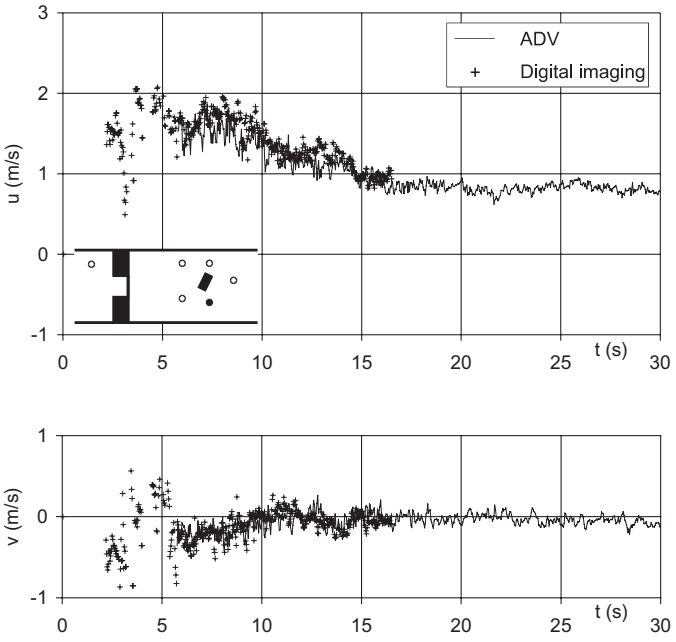

Figure 25 Gauge G4—Velocity measurements.

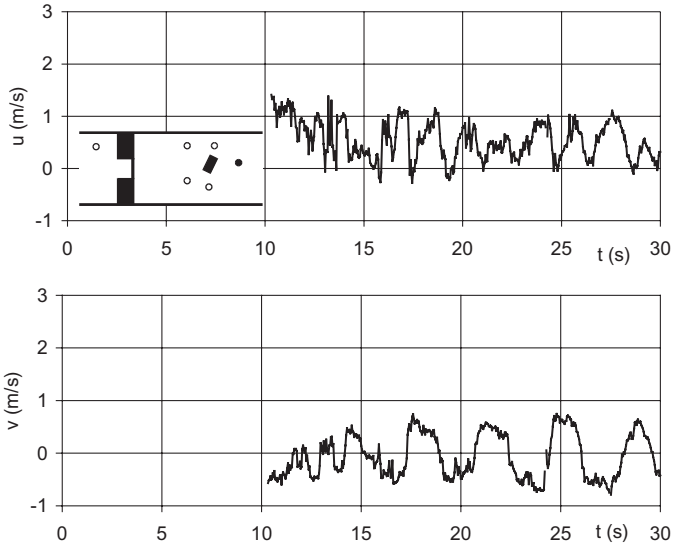

Figure 26 Gauge G5—Velocity measurements.

Finally, interesting results were obtained at gauge G5, located in the wake of the building (Fig. 26). The oscillations (periodic change in sign of the transversal velocity component v) that can be observed reveal the presence of wake eddies, which were clearly observed visually during the experiments.

6 Conclusions

A dam-break flow experiment in a channel with an obstacle was presented. Using different measurement devices, it was possible to characterise the flow in a quite complete way. Those measurements form a data set that can be used for the validation of numerical models aimed at solving fast transient flow problems in complex topographies, which was one of the aims of the IMPACT European project.

During this experimental campaign, it was also possible to show how digital imaging techniques can complete the commonly available data. Indeed, the whole field may be covered, and the method is free of any intrusion potentially affecting the measurement.

Acknowledgments

The authors wish to acknowledge the financial support offered by the European commission for the IMPACT project under the fifth framework programme (1998–2002), environment and sustainable development thematic programme, for which Karen Fabbri was the EC project officer.

The overall contribution made by the IMPACT project team is also recognised. IMPACT team member organisations comprise: HR Wallingford Ltd (UK), Universität der Bundeswehr München (Germany), Université Catholique de Louvain (Belgium), CEMAGREF (France), Università di Trento (Italy), Universidad de Zaragoza (Spain), CESI (Italy), SWECO Gröner AS (Norway), Instituto Superior Técnico (Portugal), Geo Group (Czech Republic) and H-EURAqua (Hungary).

Finally, the authors also acknowledge the help of Benoit Spinewine and Benjamin Noël in performing the experimental measurements, and wish to thank Benoit Spinewine for the treatment of the digital imaging measurements.

Appendix: List of available data

This section lists the available data that can be found in the attached DVD-ROM, and indicates under which format the data is presented.

Results at the gauging points (water depth and velocity)

The results at the six gauging points (G1, . . . , G6) are given in the text file `building_gauges.txt` with the format indicated in Table A.1. For gauges G1 to G5, both water level and velocity ADV measurements are available, while for gauge G6, only the water level was recorded. The measurements were recorded with a time step of 0.01 s.

Velocity field

The velocity field over the area around the building channel is available at the following times after the opening of the gate

Table A.1 Format of water depth and velocity data in the attached DVD-ROM

Col 1	*Col 2*	*Col 3*	*Col 4*	···	*Col 14*	*Col 15*	*Col 16*	*Col 17*
Time (s)	G1 h (m)	G1 u (m/s)	G1 v (m/s)	···	G5 h (m)	G5 u (m/s)	G5 v (m/s)	G6 h (m)
...	...	...	...	...	...	...	...	...

Table A.2 Format of the velocity-field data in the attached DVD-ROM

Col 1	*Col 2*	*Col 3*	*Col 4*
x (m)	y (m)	u (m/s)	v (m/s)
…	…	…	…

corresponding to the breaking of the dam: $t = 1\,\text{s}$, $5\,\text{s}$, $10\,\text{s}$ and $20\,\text{s}$. There are thus four files, with the format indicated in Table A.2. For example, the file `building_vel_t05.txt` gives the velocity measurements at time $t = 5\,\text{s}$.

The origin of the axes is located at the centre of the gate (see sketch in Figure 1). The values u and v are the velocity components in the x and y directions, respectively.

Notations

g = Acceleration due to gravity
h = Water depth
h_0 = Initial water depth in the reservoir
t = Time
t_{op} = Gate opening time
u = Velocity longitudinal component (in the x-direction)
u_0 = Velocity at the level z_0, measured by the ADV
u_{s} = Surface velocity
u_* = Shear velocity
v = Velocity transversal component (in the y-direction)
x = Abscissa along the channel axis, towards the downstream direction ($x = 0$ at the centre of the gate)
y = Transverse co-ordinate, towards the left bank of the channel ($y = 0$ at the centre of the gate)
z = Level
z_0 = Level of the ADV velocity measurements

References

1. CAPART, H., YOUNG, D.L. and ZECH, Y. (2002). "Voronoï Imaging Methods for the Measurements of Granular Flows". *Experiments in Fluids*, 32(21), 121–135.
2. GRAF, W.H. and ALTINAKAR, M.S. (1998). *Fluvial Hydraulics: Flow and Transport Processes in Channels of Simple Geometry.* Wiley, Chichester, UK.
3. IMPACT (2004). EC Contract EVG1-CT-2001-00037 Investigation of Extreme Flood Processes and Uncertainties, www.impact-project.net.
4. LAUBER, G. and HAGER, W. H. (1998a). "Experiments to Dam-Break Wave: Horizontal channel". *J. Hydraul. Res.* 36(3), 291–307.
5. LAUBER, G. and HAGER, W. H. (1998b). "Experiments to Dam-Break Wave: Sloping Channel". *J. Hydraul. Res.* 36(5), 761–773.
6. NOËL, B., SOARES-FRAZÃO, S. and ZECH, Y. (2003). "Computation of the 'Isolated Building Test Case' and the 'Model City Experiment' Benchmarks". In *EC Contract EVG1-CT-2001-00037 IMPACT Investigation of Extreme Flood Processes and Uncertainty, Proceedings 3rd Project Workshop, Louvain-la-Neuve*, Belgium 6–7 November 2003 (CD-ROM).
7. SOARES-FRAZÃO, S., NOËL, B., SPINEWINE, B. and ZECH, Y. (2003). "The Isolated Building Test Case: Results from the IMPACT Benchmark". In *EC Contract EVG1-CT-2001-00037 IMPACT Investigation of Extreme Flood Processes and Uncertainty, Proceedings 3rd Project Workshop, Louvain-la-Neuve*, Belgium 6–7 November 2003 (CD-ROM).
8. SOARES-FRAZÃO S., NOËL B. and ZECH Y. (2004). "Experiments of Dam-Break Flow in the Presence of Obstacles". *Proceedings River Flow 2004 Conference, Naples, Italy*, Balkema, Lisse, The Netherlands, 911–918.
9. SPINEWINE, B., CAPART, H., LARCHER, M. and ZECH, Y. (2003). "Three-Dimensional Voronoï Imaging Methods for the Measurement of Near-Wall Particulate Flows". *Experiments in Fluids*, 34(2), 227–241.
10. VISCHER, D.L. and HAGER, W.H. (1998). *Dam Hydraulics*, Wiley, Chichester, UK.